
**ELECTRONIC PROPERTIES
OF SOLID**

Temperature Dependence of the Electronic Structure of La_2CuO_4 in the Multielectron LDA+GTB Approach

I. A. Makarov* and S. G. Ovchinnikov**

Institute of Physics, Siberian Branch, Russian Academy of Sciences, Krasnoyarsk, 660036 Russia

*e-mail: macplay@mail.ru

**e-mail: sgo@iph.krasn.ru

Received November 22, 2014

Abstract—The band structure of La_2CuO_4 in antiferromagnetic and paramagnetic phases is calculated at finite temperatures by the multielectron LDA+GTB method. The temperature dependence of the band spectrum and the spectral weight of Hubbard fermions is caused by a change in the occupation numbers of local multielectron spin-split terms in the antiferromagnetic phase. A decrease in the magnetization of the sublattice with temperature gives rise to new bands near the bottom of the conduction band and the top of the valence band. It is shown that the band gap decreases with increasing temperature, but La_2CuO_4 remains an insulator in the paramagnetic phase as well. These results are consistent with measurements of the red shift of the absorption edge in La_2CuO_4 with increasing temperature.

DOI: 10.1134/S1063776115090174

1. INTRODUCTION

The complex phase diagram of HTSC cuprates is still a subject of both theoretical and experimental studies. In the normal phase, the nature of the pseudogap state is unclear. The decisive role of the spin fluctuations of the short-range antiferromagnetic (AFM) order is suggested by many results [1]. However, the authors of some recent papers underline the important role of local dynamical charge fluctuations and distortions [2–5] and the possible existence of hidden order parameters [6]. In our opinion, the problem of normal and superconducting states in HTSC cuprates has remained open almost for 30 years for the following reasons. First, all the subsystems of the crystal—electronic, magnetic and crystal lattice—are complex and interrelated. Second, the methods of the standard quantum theory of solids based on the zero approximation of noninteracting electrons followed by subsequent consideration of their interaction using perturbation theory are invalid due strong electron correlations (SEC).

The electronic structure of cuprates has been calculated by different methods taking SEC into account in the simple Hubbard model or the t – J model [7–10]. The hybrid LDA+GTB method, combining calculations in a multielectron, multiband p – d model in the generalized tight-binding (GTB) method [11] with calculation of model parameters in the ab initio LDA (Local Density Approximation) [12], takes into account both the band structure of cuprates and SEC effects. The concentration dependence of the band

structure of $\text{La}_{2-x}\text{Sr}_x\text{CuO}_4$ was described by the LDA+GTB method, and it was shown that transition from a doped Mott–Hubbard insulator at small x to a Fermi liquid system at large x involves two Lifshitz quantum transitions with a change in the Fermi surface topology [13]. According to LDA+GTB calculations [14, 15], the four hole pockets of a doped insulator centered at $(\pi/2, \pi/2)$ increase and intersect at the Brillouin zone boundary at $x_{c1} = 0.15$, and for $x > x_{c1}$, two surfaces exist around the point (π, π) . The smaller surface collapses at the point $x_{c2} = 0.24$, and for $x > x_{c2}$, only one large surface exists, which is typical of the Fermi liquid state. Qualitatively similar Fermi surfaces were also obtained at different concentrations in [8, 10]; however, the Lifshitz transitions were not discussed in these papers. Study of electronic properties near Lifshitz transitions showed that a logarithmic singularity in the density of states $N(\varepsilon_F)$ at $x = x_{c1}$ ensures the maximum temperature of the superconducting transition, while the transition at the point x_{c2} corresponds at $T = 0$ K to the transition from the pseudogap state to the Fermi liquid state [16, 17]. Both these concentrations correspond to singularities in the phase diagram: the optimal doping point (0.15) and the point of intersection of the pseudogap temperature $T^*(x)$ with the axis $T = 0$ K [18].

The strong concentration dependence of the band structure taking into account SEC appears due to the presence of the occupation numbers of local states with one or two holes in a unit cell in multielectron approaches. The occupation numbers depend not

only on the doping level but also on temperature. Therefore, the electronic structure will also depend on temperature. Experimentally, this is probably manifested in the dependence of temperature T^* on doping. The temperature dependence of the band structure of cuprates has been poorly studied theoretically. In this paper, we consider the temperature dependence of the band structure of La_2CuO_4 in antiferromagnetic and paramagnetic states. The splitting of single-hole $S = 1/2$ states over the spin projection in the AFM phase is proportional to the magnetic moment $\langle S^z \rangle$ of the sublattice and decreases with heating. We find the temperature dependence of $\langle S^z \rangle$ from the effective Heisenberg model. As temperature increases, new states in the valence and conduction bands acquire the spectral weight and dispersion. New bands that have split from the top of the valence band and the bottom of the conduction band undergo considerable changes with a further increase in T . Above T_N , the dispersion becomes similar to a paramagnetic spectrum at $T = 0$ K calculated by the LDA method [19].

In Section 2, we describe the features of the method and present the Hamiltonian of the three-band p - d model, the Green's function in general form, and the equations for its poles. In Section 3, we show the evolution of the band structure and density of states with increasing temperature and demonstrate the temperature dependence of the band gap. Section 4 presents the temperature dependences of isoenergetic surfaces obtained for different regions in the valence and conduction bands.

2. CALCULATION OF THE BAND STRUCTURE AT FINITE TEMPERATURES

We consider HTSC cuprates by the example of an undoped single-layer La_2CuO_4 compound. The electronic structure of these compounds near the Fermi level is formed by the d_x orbitals of copper and $p_{x,y}$ orbitals of oxygen in the CuO_2 plane. Therefore, we will describe interactions in this system by using the three-band Emery model,

$$\begin{aligned}
 H = & \sum_{f\sigma} \varepsilon_d d_{xf\sigma}^\dagger d_{xf\sigma} + \sum_{f\sigma} \varepsilon_p d_{f\sigma}^\dagger p_{f\sigma} \\
 & + \sum_{fg\sigma} (-1)^{R_g} t_{pd} (d_{xf\sigma}^\dagger p_{g\sigma} + \text{H.c.}) \\
 & + \sum_{fg\sigma} (-1)^{M_g} t_{pp} (p_{f\sigma}^\dagger p_{g\sigma} + \text{H.c.}) \\
 & + \sum_f U_d d_{xf\uparrow}^\dagger d_{xf\uparrow} d_{xf\downarrow}^\dagger d_{xf\downarrow} + \sum_f U_p p_{f\uparrow}^\dagger p_{f\uparrow} p_{f\downarrow}^\dagger p_{f\downarrow} \\
 & + \sum_{fg\sigma\sigma'} V_{pd} d_{xf\sigma}^\dagger d_{xf\sigma} p_{g\sigma'}^\dagger p_{g\sigma'}.
 \end{aligned} \quad (1)$$

Here, $d_{xf\sigma}$ and $p_{g\sigma}$ are the hole annihilation operators with the spin projection σ at the copper atom f and

oxygen atom g , ε_d is the on-site energy for a hole at Cu and ε_p – at O; t_{pd} is the hopping integral between d_x and p orbitals in the CuO_2 plane, t_p is the hopping integral between planar oxygen orbitals; U_d and U_p are Coulomb interactions between two holes at copper and oxygen atoms, respectively; and V_{pd} is the intersite Coulomb interaction. Coefficients R_g and M_g depend on the overlap sign of wavefunctions on copper and oxygen atoms. $R_g = 0$ for atoms $g = (g_x - a_x/2, g_y)$, $(g_x, g_y - a_y/2)$ and $R_g = 1$ for $g = (g_x + a_x/2, g_y)$, $(g_x, g_y + a_y/2)$, where a_x and a_y are lattice constants. The parameters of the Hamiltonian were calculated in [20] by the LDA+GTB method.

The GTB method involves a few stages: the exact diagonalization of the unit cell, the construction of quasiparticle excitations between the eigenstates of the cell characterized by Hubbard operators and the cluster form of perturbation theory. Hamiltonian (1) is divided into the intracluster part containing all interactions inside the CuO_4 cluster and the Hamiltonian of intercluster interactions. The diagonalization of the intracluster Hamiltonian in the bases with the numbers of holes $n_h = 0, 1, 2$ allows us to obtain exactly the local many-particle states and their energies. Since for $x = 0$ and $T = 0$, a hole propagates in the CuO_2 plane in the background of the long-range antiferromagnetic order, the local states $|1_\downarrow, i\rangle$, and $|1_\uparrow, i\rangle$ of the hole with the opposite spin projections in a cluster with $n_h = 1$ will be split (Fig. 1). The gap $2\Delta_{AF}$ between these states is determined by the molecular Weiss field $\Delta_{AF} = ZJ\langle S^z \rangle$ of the antiferromagnetic type, where Z is the number of nearest neighbors ($Z = 4$ for a CuO_2 layer) and J is the superexchange interaction strength. The superexchange interaction appears in the same initial Hamiltonian of the p - d model in second-order perturbation theory in t_{pd}/U [21], as in the Hubbard model [22]. The influence of temperature on the average value $\langle S^z \rangle$ of the spin momentum projection on the z axis can be self-consistently calculated in the mean-field approximation in the Heisenberg model from the equation

$$\langle S^z \rangle = \frac{1}{2} \tanh \frac{ZJ\langle S^z \rangle}{2k_B T}. \quad (2)$$

Note that the long-range antiferromagnetic order in HTSC cuprates is caused by the quasi-two-dimensionality of their magnetic system with the exchange integral $J_\perp \ll J$. The introduction of J_\perp in spin-wave theory makes it possible to obtain the expression $T_N \sim J/\ln(J/J_\perp)$, which tends to zero for $J_\perp \rightarrow 0$. Near the ground state, a two-sublattice magnetic structure exists. This structure determines the dispersion law of a hole in undoped cuprates. In this sense, our expression (2) specifies the method for simulating a two-sublattice structure. We can add J_\perp to this expression,

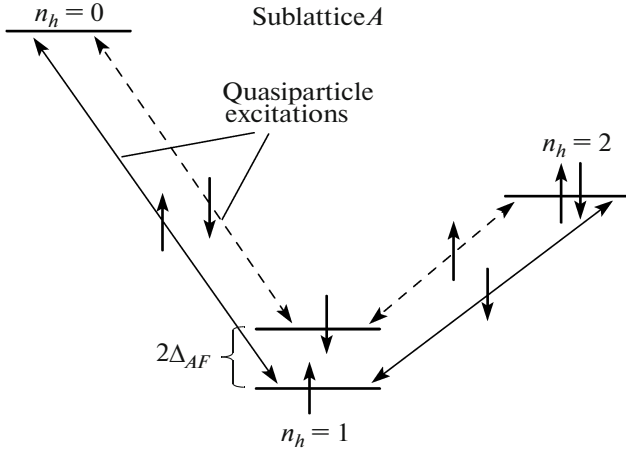


Fig. 1. Eigenstates of a CuO_4 cluster for $n_h = 0, 1, 2$ (horizontal straight lines) of sublattice A in the low-energy region. The ground states of the Hilbert space sector with $n_h = 1$ in two magnetic sublattices A and B have opposite spin momentum projections. The solid straight lines drawn between eigenstates show quasiparticle excitations with the nonzero spectral weight. The dashed straight lines show quasiparticle excitations with the zero spectral weight at $T = 0$.

but this will not result in any considerable change in the theory, and the Néel temperature $T_N \sim (4J + 2J_\perp)$ obtained from (2) is incorrect. In this paper, we do not propose a self-consistent description of the magnetic order and electronic structure. Instead, we select the value of J so that the Néel temperature in the mean-field theory would be consistent with its experimental value ($T_N = 325$ K for La_2CuO_4). This approach makes it possible to qualitatively describe the change in the electronic structure with changing magnetic order, but it cannot give the quantitative temperature dependences of the electronic structure parameters.

The occupation of hole states with opposite spin projections will depend on temperature,

$$\begin{aligned} n_{G\sigma} &= 1/2 + \eta_G(\sigma)\langle S^z \rangle, \\ \eta_A(\sigma) &= \begin{cases} 1, & \sigma = 1/2, \\ -1, & \sigma = -1/2, \end{cases} \\ \eta_B(\sigma) &= \begin{cases} 1, & \sigma = -1/2, \\ -1, & \sigma = 1/2, \end{cases} \end{aligned} \quad (3)$$

where G is the index of a sublattice (A or B) and σ is the spin projection in the one-hole state.

Transitions between the eigenstates $|p\rangle$ and $|q\rangle$ of a CuO_4 cluster with $\Delta n_h = 1$ are quasiparticle Fermi-type excitations described by Hubbard operators X_f^{pq} . Quasiparticle transitions between the $n_h = 0$ and $n_h = 1$ states form upper Hubbard band (UHB) of the electrons, which is the conduction band, while lower Hubbard band (LHB) of the electrons, which is the valence band, is formed by transitions between the

$n_h = 1$ and $n_h = 2$ states. The local quasiparticle excitations are used below as unperturbed states in constructing the cluster form of perturbation theory representing the intercluster Hamiltonian in terms of Hubbard operators. The total Hamiltonian in the representation of Hubbard operators has the form

$$\begin{aligned} H &= \sum_f \left[\sum_{q\sigma} \varepsilon_{1q\sigma} X_f^{qq} + \sum_p \varepsilon_{2p} X_f^{pp} \right. \\ &- \sum_{g \neq f} \sum_{pqmn} 2t_{pd} \mu_{fg} \gamma_{d_x}^*(pq) \gamma_b(mn) X_f^{\dagger pq} X_g^{mn} \\ &\left. - \sum_{g \neq f} \sum_{pgmn} 2t_{pp} \nu_{fg} \gamma_b^*(pq) \gamma_b(mn) X_f^{\dagger pq} X_g^{mn} \right], \end{aligned} \quad (4)$$

where $\varepsilon_{1q\sigma}$ is the energy of the one-hole $|q\rangle$ state with the spin projection σ and ε_{2p} is the energy of the two-hole $|p\rangle$ state, $\gamma_\lambda(pq) = \langle p | \lambda | q \rangle$, λ denotes either the copper d_x orbital or the molecular oxygen b_{1g} orbital. The values of structural factors μ_{fg} and ν_{fg} are given in [11].

We obtain the dispersion of quasiparticle excitations by using the equation of motion method for the Green's function $D_{fg}^{GG'}(pq; mn) = \langle \langle X_{fS}^{pq} | X_{gS'}^{mn} \rangle \rangle$, where f and g are the cells of magnetic sublattices G and G' . The total Green's function in matrix form is

$$\hat{D}_{fg} = \begin{pmatrix} D_{fg}^{AA} & D_{fg}^{AB} \\ D_{fg}^{BA} & D_{fg}^{BB} \end{pmatrix}. \quad (5)$$

The decoupling of the equation of motion for Green's function (5) is performed in the Hubbard I approximation. As a result, we obtain the Dyson equation

$$\hat{D}(\mathbf{k}) = (\hat{D}_0^{-1} - \hat{t}(\mathbf{k}))^{-1}, \quad (6)$$

where $D_0^{pq} = F(pq)/(E - \Omega(pq))$ is the local Green's function of the CuO_4 cluster with quasiparticle excitation energy $\Omega(pq)$ and diagonal elements $F_f(pq) = \langle X_f^{pp} \rangle + \langle X_f^{qq} \rangle$ of the occupation factor matrix (or end factors in the diagrammatic technique [7]) and $\hat{t}(k)$ is the hopping integral matrix $t_{pq, mn}(k) = \sum_{\lambda\lambda'} \gamma_\lambda^*(pq) t_{\lambda\lambda'}(k) \gamma_{\lambda'}(mn)$ determined by the sum of matrix elements of p - d and p - p hoppings. The poles of Green's functions (6) are determined from the equation

$$\det \left\| \delta_{pq, mn} \frac{(E - \hat{\Omega})}{\hat{F}} - \hat{t}(\mathbf{k}) \right\| = 0. \quad (7)$$

3. BAND STRUCTURE OF La_2CuO_4 AT FINITE TEMPERATURES

The band structure at $T = 0$ K is shown in Fig. 2a. Each of the Hubbard bands is formed by the dispersion

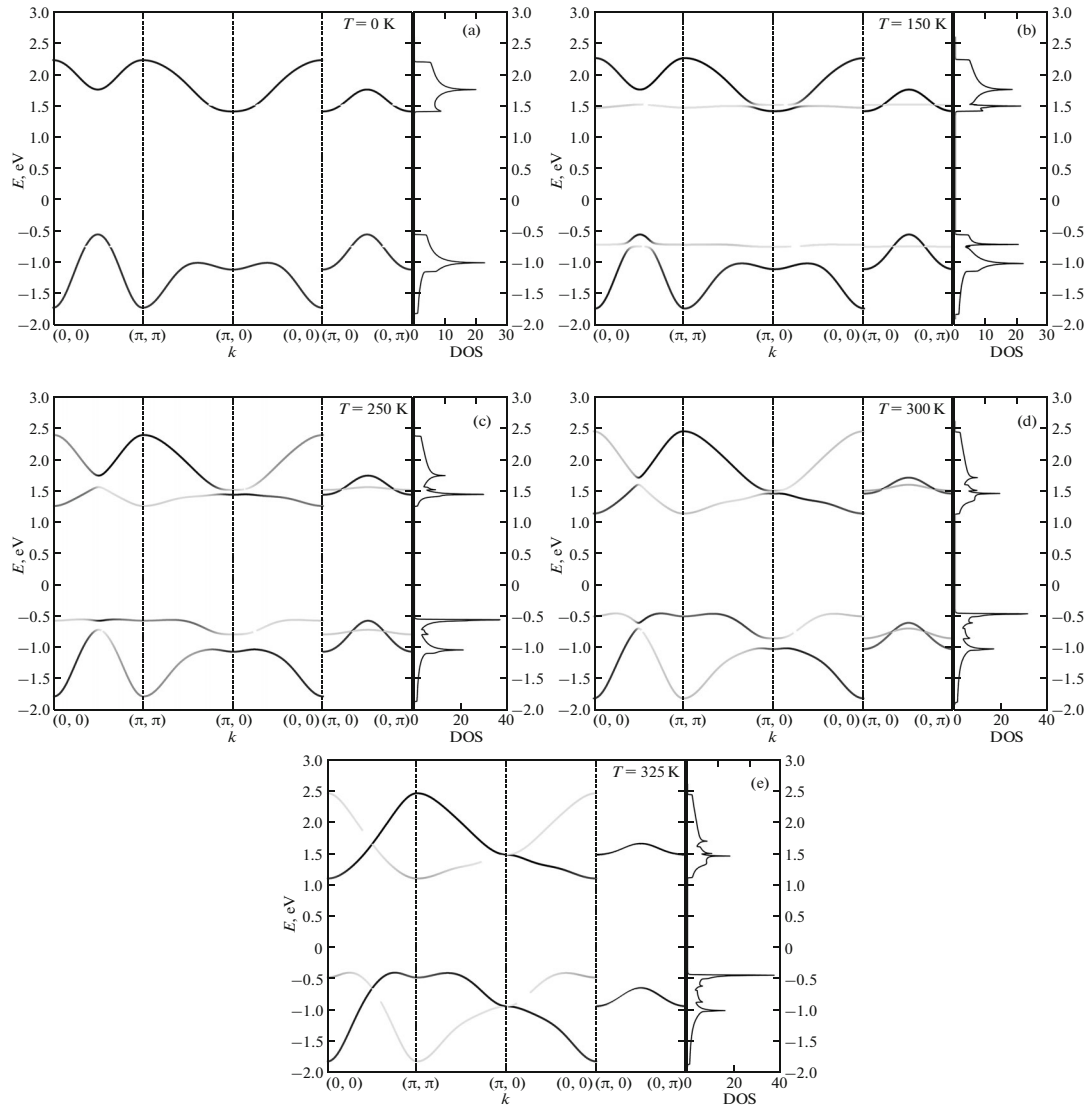


Fig. 2. Band structure and electron density of states at temperatures $T = 0$ K (a), 150 K (b), 250 K (c), 300 K (d), and 325 K (e). The spectral weight of states with different k is proportional to the line intensity.

of one quasiparticle excitation shown by solid curves in Fig. 1. The valence electron band (the hole conduction band) at $T = 0$ K has a maximum (minimum) at the point $k = (\pi/2, \pi/2)$, which is consistent with the results of earlier theoretical studies of the electronic structure of cuprates [23–26]. Because the occupation of excited one-particle states, in particular, the nearest state with the opposite spin projection, is close to zero, the quasiparticle excitations involving these states are dispersionless and their spectral intensity is zero. The spectral intensity of one-electron excitations is determined by the spectral functions of quasiparticles

$$A(k, E) = \sum_{\sigma} A_{\sigma}(k, E) \quad (8)$$

$$A_{\sigma}(k, E) = \sum_{\lambda mn} \gamma_{\lambda\sigma}^*(m) \gamma_{\lambda\sigma}(n) \text{Im} D^{mn}(k, E + i\delta).$$

Each of the spectral functions A_{σ} gives the intensity for particles with a certain spin. The dispersion of particles with opposite spin projections are identical, but they have considerably different spectral weight distributions in the Brillouin zone. At $T = 0$ K, $A_{\uparrow}(k, E)$ and $A_{\downarrow}(k, E)$ are antisymmetric with respect to the boundary of the antiferromagnetic Brillouin zone. Note that, unlike standard perturbation theory, the spectral weight of Hubbard fermions (quasiparticles) depends on the wave vector and temperature and can take fractional values.

The increase in temperature leads to two effects. First, a decrease is observed in the magnetization of sublattices and the splittings of states with opposite spin projections in each of the sublattices. Second, as temperature increases, the occupation of excited states occurs, the first excited state in the one-hole spectrum

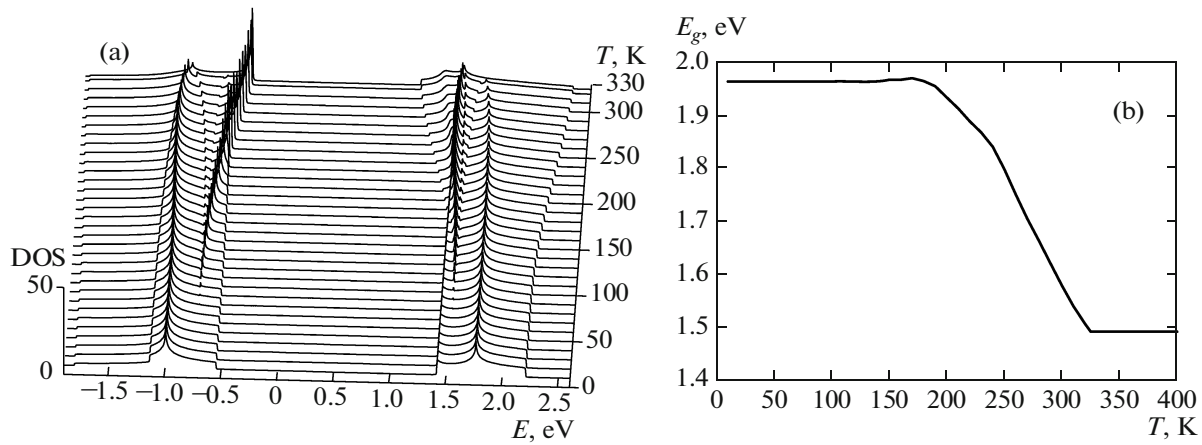


Fig. 3. Temperature dependences of the density of states (a) and the band gap E_g (b).

being the state with the spin projection opposite to its direction in the ground state. Quasiparticle transitions involving the occupied states acquire nonzero intensity and dispersion, and the interband interaction becomes possible.

These effects lead to considerable reconstruction of the band structure with increasing T . The dispersionless levels with the zero spectral weight at $T = 0$ K located within the LHB and UHB acquire the spectral weight and a weak dependence on k . The interband interactions produce splittings in the initial LHB and UHB (Fig. 2b), separating the top of the valence band and the bottom of the conduction band from broad Hubbard bands. The splitting is manifested in the density of states in the form of additional peaks. Note that at any temperature up to the magnetic phase transition, there exist two points at the boundary of the antiferromagnetic Brillouin zone at which the dispersion surfaces of the split bands are touching.

As temperature further increases, splittings increase and the width of the subbands of the top of the valence band and the bottom of the conduction band decreases. For the top of the valence band, the largest spectral weight corresponds to the states of the flat band in the region $(\pi/2, \pi/2) - (\pi, \pi)$, while for the conduction band, in the regions $(0, 0) - (\pi/2, \pi/2)$ and $(\pi, 0) - (0, 0)$. Near $T = 238$ K, the narrow band “reverses” (Fig. 2c) so that the local maximum of the valence band at $k = (\pi/2, \pi/2)$ transforms to the local minimum, while in the conduction band, on the contrary, the minimum at $k = (\pi, 0)$ transforms to the maximum (Fig. 2d). Such changes occur due to the tendency to dispersion degeneracy at the points of the k space on the antiferromagnetic Brillouin zone boundary, at the point of transition to the paramagnetic phase. For $T = T_N$, the one-hole states with both spin projections become equally probable and the band structure takes the form typical for the paramagnetic phase with maxima in the vicinity of $k = (\pi, \pi)$ (Fig. 2e). Figures 2a–2e well demonstrate the redistribu-

tion of the spectral weight with temperature from the initial antiferromagnetic band to the paramagnetic band with the formation of a weak shadow band.

The transformation of the top of the valence band and the bottom of the conduction band with increasing temperature is naturally accompanied by a change in the density of states. Above 90 K, new peaks appear in the valence and conduction bands (Fig. 3a). The intensity of these peaks increases with temperature. In addition, the width of both bands and the width of the band gap E_g change. In the interval from zero to 170 K, the gap width slightly increases due to the approach of one-hole levels with different spins. At $T > 170$ K, the energy of quasiparticles in the conduction band with wave vectors close to $k = (0, 0)$ decreases and the spectral weight transfers to them. In contrast, the energy of the top of the valence band increases. All this leads to a decrease in the band gap width (Figs. 3a, 3b). The minimum value of E_g is achieved in the paramagnetic phase. Nevertheless, the band gap remains open in the entire temperature interval from 0 to T_N and far above, because its width is determined by the charge-transfer energy $\Delta = \varepsilon_p - \varepsilon_d$ and the interatomic Coulomb interaction V_{pd} . Thus, the state of charge-transfer insulator is preserved in the AFM and PM phases, unlike band approaches with the formation of a gap due to the appearance of a spin-density wave (SDW) or LDA+U, where the band gap is also formed due to spin splitting. In the SDW and LDA+U scenarios, a metal state should be observed at higher temperatures, which contradicts experiments with La_2CuO_4 .

The earlier measurements of the reflectivity and ε_2 spectra in an undoped La_2CuO_4 compound revealed a red shift of the peak corresponding to the charge transfer between the Zhang–Rice singlet and UHB with increasing temperature [27–29]. As temperature increased from 122 K to 447 K, the peak of ε_2 shifted to lower energies by 0.22 eV [27]. Our calculations predicted a 0.47 eV decrease in the band gap width ΔE in this temperature range. This small discrepancy can be

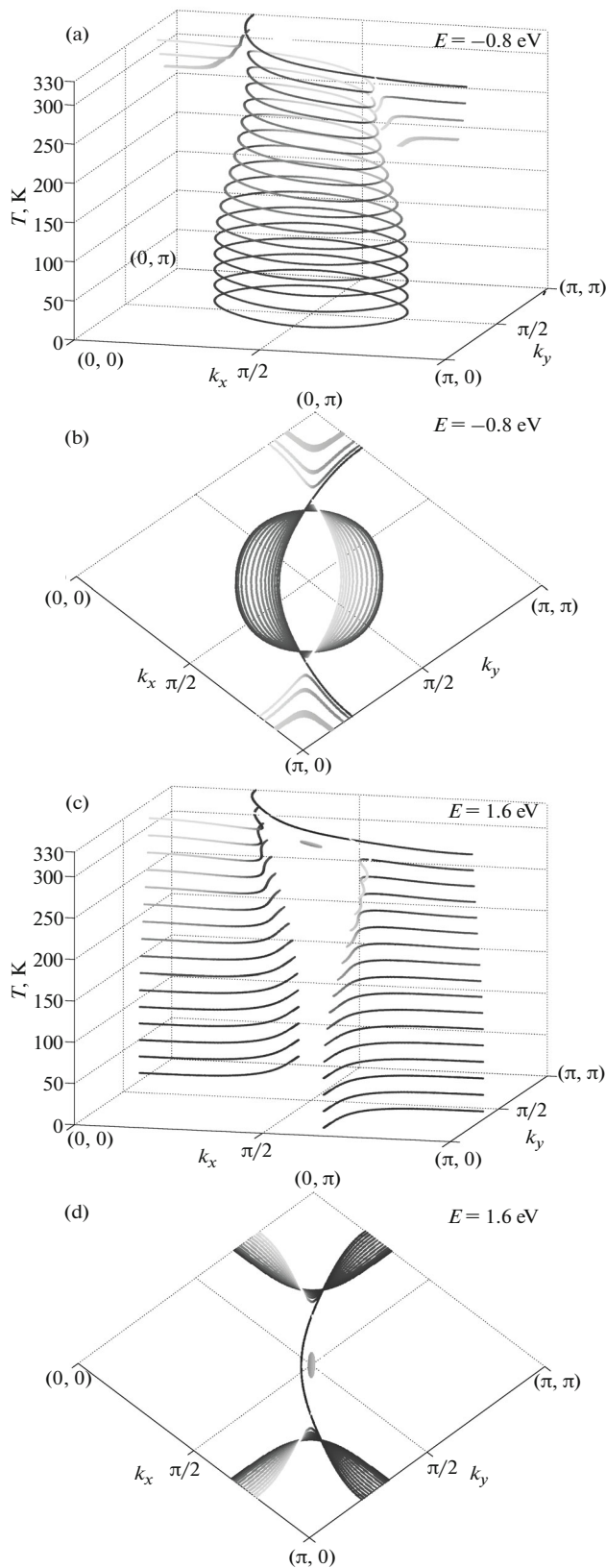


Fig. 4. Transformation of the isoenergetic contour with temperature changing from 10 to 325 K for the valence band (a, b: top view) and the conduction band (c, d: top view).

explained by the influence of temperature on the electronic structure via other mechanisms. Such mechanisms include the dependence of the interaction parameters in the system on the temperature expansion of the crystal lattice [29], the temperature dependence of the electron–phonon interaction, and polarization effects. However, without question, the reconstruction of the electronic structure caused by the decrease in the magnetization of sublattices with increasing temperature leads, to a great extent, to a decrease in the interband excitation energy.

4. EVOLUTION OF ISOENERGETIC CONTOURS WITH INCREASING TEMPERATURE

Calculation of the temperature dependence of the Fermi surface in a doped cuprate is a separate problem that is not considered here. Nevertheless, this evolution can be estimated qualitatively in the rigid model approximation, as was done at $T = 0$ K in [30]. Figure 4a shows the cross sections of the dispersion surface at an energy of $E = -0.8$ eV. One can see that at temperatures up to 260 K, these cross sections have the form of hole pockets centered at $k = (\pi/2, \pi/2)$. Fermi surfaces in the form of hole pockets are inherent in weakly doped p -type compounds, which is confirmed by ARPES experiments [31] and experiments with quantum oscillations [32–34]. The size of pockets decreases with increasing temperature. At $T > 260$ K, low-intensity electron pockets appear around points $k = (\pi, 0)$ and $k = (0, \pi)$. Simultaneously, the hole pockets cease to decrease in size and begin to extend to electron pockets. The spectral weight of hole and electron pockets transfers from one side to another so that when hole and electron pockets join at the magnetic phase transition point $T = T_N$, a large hole contour remains around $k = (\pi, \pi)$. In addition, a shadow hole contour centered at point $k = (0, 0)$ is also present; its intensity, however, is very weak. The Fermi surface upon electron doping is determined by the isoenergetic contours obtained by the cross section of the dispersion surface in the conduction band. In the case of $E = 1.6$ eV, the isoenergetic contour at $T = 0$ has the form of two electronic pockets around $k = (\pi, 0)$ and $k = (0, \pi)$, which is consistent with the Fermi surface in ARPES for a weakly doped n -type $\text{Nd}_{2-x}\text{Ce}_x\text{CuO}_4$ compound [35]. As temperature increases, these pockets extend to the point $k = (\pi/2, \pi/2)$. In the vicinity of T_N , a hole pocket appears centered at $k = (\pi/2, \pi/2)$. The obtained section qualitatively replicates the Fermi surface of optimally doped cuprates in ARPES experiments with $\text{Nd}_{2-x}\text{Ce}_x\text{CuO}_4$ [35] and $\text{Sm}_{2-x}\text{Ce}_x\text{CuO}_4$ [36] and in calculations of ARPES spectra [37]. At the phase transition point, two electronic pockets and one hole pocket are transformed into one large electronic contour around $k = (\pi, \pi)$. Similar evolutions of the Fermi surface with doping and temperature are explained by the fact that both

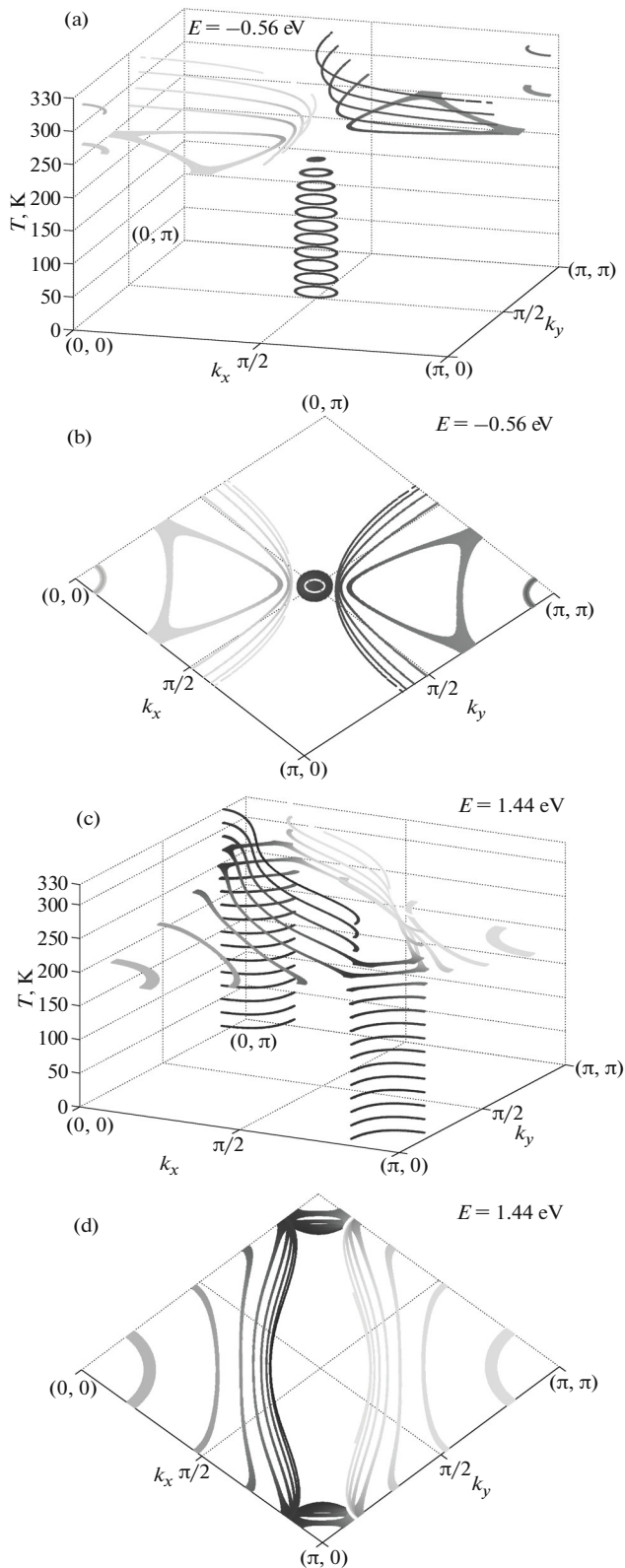


Fig. 5. Transformation of the isoenergetic contour with temperature for energy near the top of the valence band (a, b: top view) and the bottom of the conduction band (c, d: top view).

these factors change the spin gap width and the population of the ground and excited states. In the case of doping, additional carriers destroy spin correlations and produce a redistribution of the spectral weight among the bands formed by excited states.

The evolution of the isoenergetic contour will be different for different regions of the dispersion surface. Figures 5a and 5b show the change in the isoenergetic contour near the top of the valence band. The contour of the dispersion surface cross section at an energy of $E = -0.56$ eV is formed by the separated narrow sub-band with dispersion different from that of the main band. At $T < 230$ K, there exists a small hole pocket around $k = (\pi/2, \pi/2)$ (Figs. 5a, 5b). The pocket closes at $T = 230$ K, and then until $T = 240$ K, the cross section is in the band gap. In the interval 240 K $< T < 250$ K, two hole pockets with different intensities and centers located between points $k = (0, 0)$, $(\pi/2, \pi/2)$, and (π, π) transform to large hole pockets and two small electronic pockets around $k = (0, 0)$ and $k = (\pi, \pi)$.

The cross section of the dispersion surface in the bottom of the conduction band at the energy $E = 1.44$ eV also demonstrates a completely different temperature dependence (Figs. 5c, 5d). At $T < 190$ K, isoenergetic contours represent electronic pockets around antinodal points $k = (\pi, 0)$ and $k = (0, \pi)$. Above 190 K, electronic pockets around $k = (0, 0)$ and $k = (\pi, \pi)$ are added to them, which first simply increase in size and then at $T = 230$ K change their shape and curvature. At $T = 250$ K, the electronic pockets merge, thereby forming a hole pocket around $k = (\pi/2, \pi/2)$. The hole pocket grows and transforms after $T = 280$ K to two electronic contours around $k = (0, 0)$ and $k = (\pi, \pi)$.

5. CONCLUSIONS

We have described the temperature dependence of the undoped single-layer La_2CuO_4 cuprate by the LDA+GTB method. As temperature increases, the average spin momentum of the unit cell and the spin gap between local one-particle states with opposite spin projections decrease, while the population of excited states increases. As a result, both the spin ordering and band structure change with increasing temperature. The reconstruction of the electronic structure involves the formation of new bands at the top of the valence band and bottom of the conduction band, the redistribution of the spectral weight, and a change in the band and band gap widths. The magnetic phase transition from the antiferromagnetic state to the paramagnetic state is accompanied by transformation of the LHB and UHB with maxima at point $k = (\pi/2, \pi/2)$ to pairs in high-intensity and shadow bands with maxima in the vicinity of point $k = (\pi, \pi)$ and $k = (0, 0)$. Despite the decrease in the band gap width, it remains open in the entire temperature range from zero to T_N and above. Thus, the La_2CuO_4 com-

pound remains a insulator with a change in its magnetic state.

ACKNOWLEDGMENTS

The work was supported by the Russian Science Foundation (project no. 14-12-00061).

REFERENCES

1. M. V. Sadovskii, Phys.—Usp. **44** (5), 515 (2001).
2. J. Chang, E. Blackburn, A. T. Holmes, N. B. Christensen, J. Larsen, J. Mesot, Ruixing Liang, D. A. Bonn, W. N. Hardy, A. Watenphul, M. V. Zimmermann, E. M. Forgan, and S. M. Hayden, Nat. Phys. **8**, 871 (2012).
3. G. Ghiringhelli, M. Le Tacon, M. Minola, S. Blanco-Canosa, C. Mazzoli, N. B. Brookes, G. M. De Luca, A. Frano, D. G. Hawthorn, F. He, T. Loew, M. Moretti Sala, D. C. Peets, M. Salluzzo, E. Schierle, et al., Science (Washington) **337**, 821 (2012).
4. E. Blackburn, J. Chang, A. H. Said, B. M. Leu, Ruixing Liang, D. A. Bonn, W. N. Hardy, E. M. Forgan, and S. M. Hayden, Phys. Rev. B: Condens. Matter **88**, 054506 (2013).
5. R. Comin, A. Frano, M. M. Yee, Y. Yoshida, H. Eisaki, E. Schierle, E. Weschke, R. Sutarto, F. He, A. Soumyanarayanan, Yang He, M. Le Tacon, I. S. Elfimov, Jennifer E. Hoffman, G. A. Sawatzky, et al., Science (Washington) **343**, 390 (2014).
6. C. M. Varma, Phys. Rev. B: Condens. Matter **55**, 14554 (1997); C. M. Varma, Nature (London) **468**, 184 (2010).
7. R. O. Zaitsev, Sov. Phys. JETP **43** (3), 574 (1976).
8. A. F. Barabanov, A. A. Kovalev, O. V. Urazaev, A. M. Belemuk, and R. Hayn, J. Exp. Theor. Phys. **92** (4), 677 (2001).
9. V. V. Val'kov and D. M. Dzebisashvili, J. Exp. Theor. Phys. **100** (3), 608 (2005).
10. N. M. Plakida and V. S. Oudovenko, J. Exp. Theor. Phys. **104** (2), 230 (2007).
11. V. A. Gavrichkov, S. G. Ovchinnikov, A. A. Borisov, and E. G. Goryachev, J. Exp. Theor. Phys. **91** (2), 369 (2000).
12. M. M. Korshunov, V. A. Gavrichkov, S. G. Ovchinnikov, Z. V. Pchelkina, I. A. Nekrasov, M. A. Korotin, and V. I. Anisimov, J. Exp. Theor. Phys. **99** (3), 559 (2004).
13. I. M. Lifshits, Sov. Phys. JETP **11**, 1130 (1960).
14. M. M. Korshunov and S. G. Ovchinnikov, Eur. Phys. J. B **57**, 271 (2007).
15. S. G. Ovchinnikov, M. M. Korshunov, and E. I. Shneider, J. Exp. Theor. Phys. **109** (5), 775 (2009).
16. S. G. Ovchinnikov, E. I. Shneyder, and M. M. Korshunov, J. Phys.: Condens. Matter **23**, 045701 (2011).
17. E. I. Shneider, S. G. Ovchinnikov, M. M. Korshunov, and S. V. Nikolaev, JETP Lett. **96** (5), 349 (2012).
18. T. Yoshida, M. Hashimoto, and S. Ideta, Phys. Rev. Lett. **103**, 037004 (2009).
19. V. A. Gavrichkov, A. A. Borisov, and S. G. Ovchinnikov, Phys. Rev. B: Condens. Matter **64**, 235124 (2001).
20. M. M. Korshunov, V. A. Gavrichkov, S. G. Ovchinnikov, I. A. Nekrasov, Z. V. Pchelkina, and V. I. Anisimov, Phys. Rev. B: Condens. Matter **72**, 165104 (2005).
21. V. A. Gavrichkov and S. G. Ovchinnikov, Phys. Solid State **50** (6), 1081 (2008).
22. L. N. Bulaevskii, E. L. Nagaev, and D. I. Khomskii, Sov. Phys. JETP **27** (5), 836 (1968).
23. K. J. von Szczepanski, P. Horsch, W. Stephan, and M. Ziegler, Phys. Rev. B: Condens. Matter **41**, 2017 (1990).
24. D. Poilblanc and E. Dagotto, Phys. Rev. B: Condens. Matter **42**, 4861 (1990).
25. A. F. Barabanov, R. O. Kuzian, and L. A. Maksimov, J. Phys.: Condens. Matter **3**, 9129 (1991).
26. R. O. Kuzian, R. Hayn, A. F. Barabanov, and L. A. Maksimov, Phys. Rev. B: Condens. Matter **58**, 6194 (1998).
27. J. P. Falck, A. Levy, M. A. Kastner, and R. J. Birgeneau, Phys. Rev. Lett. **69**, 1109 (1992).
28. M. A. Kastner, R. J. Birgeneau, G. Shirane, and Y. Endoh, Rev. Mod. Phys. **70**, 897 (1998).
29. H. S. Choi, Y. S. Lee, T. W. Noh, Yunkyu Bang, and Y. J. Kim, Phys. Rev. B: Condens. Matter **60**, 4646 (1999).
30. L. Hozoi, M. S. Laad, and P. Fulde, Phys. Rev. B: Condens. Matter **78**, 165107 (2008).
31. J. Meng, G. Liu, W. Zhang, L. Zhao, H. Liu, X. Jia, D. Mu, S. Liu, X. Dong, J. Zhang, W. Lu, G. Wang, Y. Zhou, Y. Zhu, and X. Wang, et al., Nature (London) **462**, 335 (2009).
32. N. Doiron-Leyraud, C. Proust, D. LeBoeuf, J. Levallois, J.-B. Bonnemaïson, R. Liang, D. A. Bonn, W. N. Hardy, and L. Taillefer, Nature (London) **447**, 565 (2007).
33. E. A. Yelland, J. Singleton, C. H. Mielke, N. Harrison, F. F. Balakirev, B. Dabrowski, and J. R. Cooper, Phys. Rev. Lett. **100**, 047003 (2008).
34. A. F. Bangura, J. D. Fletcher, A. Carrington, J. Levallois, M. Nardone, B. Vignolle, P. J. Heard, N. Doiron-Leyraud, D. LeBoeuf, L. Taillefer, S. Adachi, C. Proust, and N. E. Hussey, Phys. Rev. Lett. **100**, 047004 (2008).
35. N. P. Armitage, F. Ronning, D. H. Lu, C. Kim, A. Damascelli, K. M. Shen, D. L. Feng, H. Eisaki, Z.-X. Shen, P. K. Mang, N. Kaneko, M. Greven, Y. Onose, Y. Taguchi, and Y. Tokura, Phys. Rev. Lett. **88**, 257001 (2002).
36. S. R. Park, Y. S. Roh, Y. K. Yoon, C. S. Leem, J. H. Kim, B. J. Kim, H. Koh, H. Eisaki, N. P. Armitage, and C. Kim, Phys. Rev. B: Condens. Matter **75**, 060501(R) (2007).
37. B. Valenzuela and E. Bascones, Phys. Rev. B: Condens. Matter **78**, 174522 (2008).

Translated by M. Sapozhnikov